Iranian Journal of Medical Physics

ijmp.mums.ac.ir

Dose Verification in Lung Radiotherapy Using PET Imaging of Nanoparticle-Induced Positrons

Omid Abouie Mehrizi[1], Roghiye Bodaghi Hosseinabadi[2], Asra Sadat Talebi[3,*]

1. Student Research Committee, Tabriz University of Medical Sciences, Tabriz, Iran
2. Department of Medical Physics, Hamadan University of Medical Sciences, Hamadan, Iran
3. Department of Medical Physics, Medical School, Tabriz University of Medical Sciences, Tabriz, Iran

ARTICLE INFO

Article type:
Original Paper

Article history:
Received: Oct 12, 2025
Accepted: Dec 30, 2025

Keywords:
PET
Dosimetry
Radiation Therapy
Nanoparticle
Monte Carlo

ABSTRACT

Introduction: Accurate verification of radiation dose delivery remains a major challenge in radiotherapy. Positron emission tomography (PET) imaging of megavoltage (MV)-induced positrons (MVIPET) has recently emerged as a potential in vivo dosimetry technique. In this study, we investigated the feasibility of enhancing MVIPET signals using high-Z nanoparticles (NPs), specifically platinum (Pt) and silver (Ag), to enable real-time dose monitoring during lung radiotherapy.

Material and Methods: PET images arising from positrons induced by platinum and silver nanoparticles in a lung tumor were generated during radiotherapy with 6, 10, and 15 MV photon beams using the GATE Monte Carlo code. The resulting images were evaluated for both image quality and dose verification.

Results: Results showed that positron production, absorbed dose, and PET signal intensity increased with both photon beam energy and NP concentration, with PtNPs producing significantly higher enhancement than AgNPs. High-quality MVIPET images with acceptable SBR and CNR, and low RMSE, were obtained for PtNP concentrations ≥8 wt% at 10 MV and ≥4 wt% at 15 MV. In contrast, AgNPs required higher concentrations and only yielded reliable monitoring at 15 MV. At 6 MV, image quality and dose–image correlation were insufficient for clinical feasibility.

Conclusion: These findings demonstrate that MVIPET, particularly when combined with PtNPs and higher photon energies, is a promising strategy for real-time, non-invasive dose verification in lung radiotherapy.

► *Please cite this article as:*
Abouie Mehrizi O, Bodaghi Hosseinabadi R, Talebi AS. Dose Verification in Lung Radiotherapy Using PET Imaging of Nanoparticle-Induced Positrons. Iran J Med Phys 2025; 22 (6): 369-376. 10.22038/ijmp.2026.92153.2636.

Introduction

Radiation therapy (RT) remains a crucial method for cancer treatment, with ongoing advancements in techniques and technology. These advancements aim to boost the effectiveness of treatments, increase survival rates, and improve the overall quality of life for patients with cancer [1]. The outcome of RT is directly affected by the dose delivered to the patient . Factors such as setup errors, organ motion, and anatomical changes during treatment can significantly impact the accuracy of the delivered dose to the target [2]. To address these challenges, controlling target motion and monitoring the delivered dose during treatment are essential. Target movements can be managed using strategies like respiratory motion management and image-guided radiotherapy (IGRT) [3, 4]. However, finding established commercial techniques for real-time dose monitoring in RT remains challenging. In this context, in vivo dosimetry methods have been explored. Emerging in vivo dosimetry methods, such as Cherenkov luminescence imaging and X-ray acoustic computed tomography (XACT), provide real-time feedback on dose delivery during treatment [5, 6]. However, limitations such as limited dose information near the skin surface for Cherenkov radiation and a poor signal-to-noise ratio (SNR) for XCAT limit their use for deeper targets [7-9].

Recently, positron emission tomography (PET) imaging has provided in vivo monitoring and verification of the dose delivered in proton therapy. These images are obtained from proton-induced positron emitter distributions during or immediately after treatment [10]. Conceptually, this approach can be extended to positrons induced by megavoltage (MV) photon beams. However, few studies have investigated the use of MV-Induced Positron Emission (MVIPE). Brivio et al. conducted a preliminary study to evaluate the feasibility of the MVIPE method [11]. Sheng et al. demonstrated that pair production can generate positrons suitable for dose monitoring [12].

In recent years, the application of nanoparticles (NPs) in radiotherapy has been widely studied [13-15]. High-atomic-number (high-Z) NPs have emerged as the most promising contrast agents in medical imaging due to their remarkable features, including high surface-to-volume ratios and optical, magnetic, antibacterial, and mechanical properties [16-19]. In

*Corresponding Author: Tel: 0914 782 7590; Email: Asra.talebi@yahoo.com

the presence of NPs during a megavoltage photon beam, dose monitoring can be achieved via PET imaging of positrons generated in the medium by interactions between the NPs and the beam. The pair-production cross-section depends on the atomic number of the medium. Therefore, when NPs with higher atomic numbers than the surrounding medium are present, a certain number of induced positrons are generated within the medium. The flux of 511 keV annihilation photons influences the intensity of the obtained PET images. The proportional relationship between image intensity and absorbed dose, dependent on photon fluence, establishes a correlation between MVIPET image intensity and the absorbed dose distribution. This correlation suggests that the MVIPET method could enable real-time dose monitoring during radiation therapy [20].

The primary aim of this work is to acquire MVIPET images using pair-production signals generated by MV beams in the presence of silver (Ag) and platinum (Pt) NP within a lung tumor during RT. This study uses the GATE Monte Carlo simulation code. The study investigated the effect of NP concentration and photon beam energy on the quality and quantity of the images. Additionally, the feasibility of real-time dose monitoring using MVIPET images was assessed by comparing the dose obtained from Monte Carlo simulations with that derived from PET images.

Materials and Methods

This study was conducted with the GATE 9.2 Monte Carlo toolkit. GATE, the Geant4 Application for Tomographic Emission, is an open-source simulation platform dedicated to MC simulation in medical physics. This toolkit is used in various application domains, including medical imaging, RT, and dosimetry calculations [21]. Photons and electrons were tracked using the Livermore physics model. This package covers a wide range of electron and photon interactions within an energy range from 200 eV to 100 GeV. All interactions were considered with 0.1 mm range production cuts. This value is smaller than the phantom voxels, which ensures an accurate dose estimate. Image reconstruction was performed using CASToR software, employing an ordered subset expectation maximization (OSEM) algorithm [22, 23].

Dosimetry calculation

A 1.5 cm-radius tumor was modeled in the lung of the adult male XCAT phantom (with a matrix size of 240×240×540 and voxel dimensions of 3×3×3 mm³) [24]. The tumor was assumed to be located in the lower lobe of the right lung and contained a uniform mixture of platinum (Pt) and silver (Ag) atoms distributed as NPs. Five levels of NP concentration were studied: 2, 4, 6, 8, and 10% by weight. The tumor was uniformly irradiated with 6, 10, and 15 MV photon beams, a commonly used energy range in RT. The photon beam spectrum used in this study was also derived from Sheikh-Bagheri's research [25]. The photon beam source was modeled as a disk with a radius of 1.5 cm, positioned 100 cm from the tumor center. The tumor's absorbed dose was calculated in the presence and absence of PtNPs and AgNPs at varying concentrations. The three-dimensional (3D) dose distribution was used to obtain a normalized dose-volume histogram (nDVH), which is considered the reference nDVH [26]. To ensure an uncertainty of less than 2% in the dose calculation, 2×10^8 histories were considered.

MVIPET Imaging

The PET subsystem of the RefleXion X1 machine (RefleXion Medical, Inc., Hayward, CA) was used, as described in a previously published modeling and validation study [27]. MVIPET images were acquired at various NP concentrations. Ordered Subset Expectation Maximization (OSEM) was used to reconstruct images by incorporating point-spread function (PSF) and time-of-flight (TOF) models. The OSEM reconstruction parameters of 12 iterations, 3 subsets, and 7.8 mm Gaussian filtering were adopted from a previously published study, where they were established as optimal [28]. All images were reconstructed using these parameters. In all acquired PET images, the pixel counts within the tumor region were calculated, and normalized intensity-volume histograms (nIVHs) were generated for the tumor.

Real-time Radiation Dose Monitoring

To assess the feasibility of real-time dosimetry during radiation therapy using MVIPET images, nIVHs and nDVHs were compared. The Root Mean Square Error (RMSE) statistical metric was utilized to assess the correlation between the dose derived from MVIPET images and the reference dose, that is, $RMSE = \sqrt{\frac{\sum_{20}^{80}(I_x - D_{x,ref})^2}{60}}$. Where I_x and $D_{x,\ ref}$, represent the normalized intensities at x% volume coverage from the image-based nIVH and reference nDVH, respectively [29]. Following the approach outlined in Siman et al., RMSE threshold values between x=20 and x=80 were used to minimize noise effects on the nIVH [28]. To quantitatively evaluate the images, the Contrast-to-Noise Ratio (CNR) and Signal-to-Background Ratio (SBR) were computed using the following formulas:

$$CNR = \frac{M_T - M_B}{\sigma_B} \quad (1)$$

$$SBR = \frac{M_T}{M_B} \quad (2)$$

The mean pixel intensities for the tumor and background regions are denoted as M_T and M_B, respectively. The standard deviation of the background pixel intensities is represented by σ_B. The number of histories was set to 3×10^9 to acquire the MVIPET images, ensuring an uncertainty of less than 2%.

Results

Figure 1a shows the number of produced positrons in the tumor when NPs are present at different concentrations of PtNP and AgNP. Figure 1b reveals the mean energy of

the positrons as a function of NP concentrations. As shown, increasing the energy of the MV photon beams and the concentration of NPs results in a significant increase in the number of positrons produced within the tumor. Nevertheless, the mean energy of the positrons remains consistent across concentrations. Figure 2 depicts variations in the tumor's mean absorbed dose as a function of PtNPs and AgNPs concentrations. With an increase in the concentration, the mean absorbed dose also rises for all energies. For PtNPs under a 6 MV beam, the mean dose increased by 1.7%, 5.2%, 7%, 10.5%, and 12.3% at concentrations of 2, 4, 6, 8, and 10 wt%, respectively, compared to the case without NPs. This increase was observed at 10 and 15 MV. The increases for the 10 MV beam were 3.5%, 7%, 8.7%, 12.3%, and 14%; similarly, the corresponding values for the 15 MV beam were 3.4%, 6.9%, 8.6%, 12%, and 15.5%, respectively, compared to those without PtNPs. For the 6 MV beam, the tumor's mean absorbed dose increased by 1.7%, 3.5%, and 5.2% at AgNP concentrations of 2%, 8%, and 10 wt%, respectively, compared to the NP-free condition. At 4 wt% and 6 wt%, the increases were consistently 1.7%. The dose enhancement for the 10 MV beam at the same concentrations was 1.7%, 3.5%, 5.2%, 7%, and 8.7%, respectively. Similarly, for the 15 MV beam, the dose enhancements at the corresponding concentrations were 1.7%, 5.2%, 6.9%, 8.6%, and 10.3%.

The optimal parameters were applied to reconstruct all MVIPET images, and the nIVHs were derived from these reconstructed images. Figures 3 and 4 show the counts of random, scattered, and true coincidences in the MVIPET images as a function of PtNP and AgNP concentrations. As the concentration of NPs and the incident photon energy increased, the counts for all types of coincidences also exhibited a noticeable increase. For the 6 MV beam, the number of true coincidences in the presence of PtNPs was approximately 1.06, 1.12, 1.17, 1.21, and 1.24 times higher at concentrations of 2 wt%, 4 wt%, 6 wt%, 8 wt%, and 10 wt%, respectively, compared to AgNPs. When using the 10 MV beam, the increase in true coincidences in the presence of PtNPs compared to AgNPs was 4%, 9%, 13%, 16%, and 19% higher at concentrations of 2 wt%, 4 wt%, 6 wt%, 8 wt%, and 10 wt%, respectively. Similarly, for the 15 MV beam, the increase in true coincidences for PtNPs compared to AgNPs was approximately 4%, 8.4%, 12%, 15%, and 18% higher, respectively, at the same concentrations.

Figure 5 presents the CNR and SBR of images as functions of PtNP and AgNP concentrations. For a 6 MV photon beam, NP concentration variations, whether PtNPs or AgNPs, did not significantly affect the SBR and CNR values. However, as the photon energy increased, especially in the presence of PtNPs, both SBR and CNR values showed marked improvement. In contrast, the presence of AgNPs did not produce acceptable results for the 10 MV photon beam. For tumors with PtNPs at 10 MV, the SBR and CNR values were about 4.72 and 4.8 times higher than those without PtNPs at 8 wt% and 10 wt%, respectively. For the 15 MV photon beam, the presence of PtNPs led to significant improvements in both Signal-to-Background Ratio (SBR) and Contrast-to-Noise Ratio (CNR) values as the NP concentration increased. Specifically, the SBR values increased by approximately 2.30, 2.37, 2.54, and 2.54 at PtNP concentrations of 4 wt%, 6 wt%, 8 wt%, and 10 wt%, respectively. For tumors with AgNPs at 15 MV, SBR values were approximately 2.45, 2.52, and 2.52 times higher at 6 wt%, 8 wt%, and 10 wt% concentrations, respectively, compared to tumors without AgNPs. Similarly, CNR values increased by 3.51, 3.64, and 3.84 times at the same concentrations, respectively, compared to the control without AgNPs.

Figure 6 shows how the RMSE changes as a function of PtNP and AgNP concentrations. The RMSE values for the 6 MV beam were relatively high, indicating that the MVIPET imaging method was less effective at accurately detecting the tumor in this case. The lowest RMSE was observed when the lung tumor, with a PtNP concentration of 10 wt%, was irradiated with a 15 MV beam, suggesting improved alignment between the nDVH and nIVH under these conditions. Additionally, RMSE values within an acceptable range were achieved at 8 wt% and 10 wt% PtNP concentrations when using the 10 MV beam. Concentrations exceeding 6 wt% were sufficient to achieve low RMSE values in the presence of AgNPs within the tumor when using a 15 MV photon beam. Figures 7, 8, and 9 compare the nDVH obtained through Monte Carlo simulations with the nIVH derived from MVIPET images of lung tumors containing various concentrations of PtNP and AgNP. These curves represent the data for photon energies and NP concentrations that exhibited adequate SBR and CNR values in the MVIPET images. RMSE was computed to evaluate the histogram differences

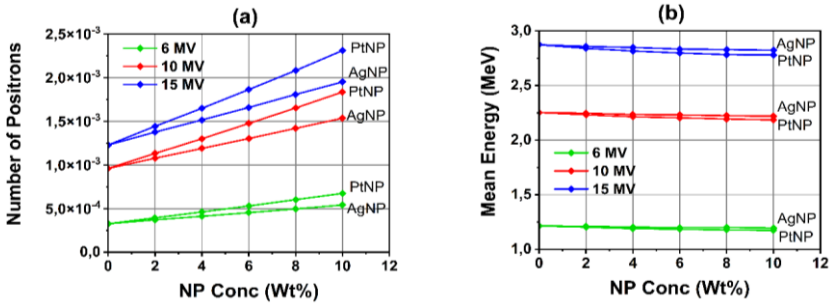

Figure 1. (a) The number of positrons per one photon, (b) the mean energy of positrons in a lung tumor as a function of PtNP and AgNP concentrations

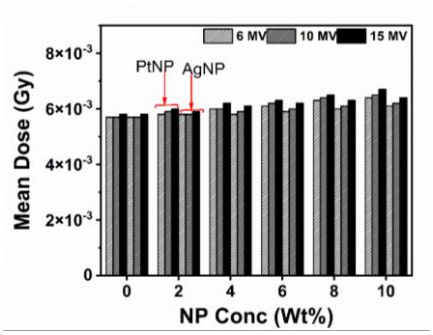

Figure 2. The mean dose (Gy per one photon) in a lung tumor as a function of PtNP and AgNP concentrations

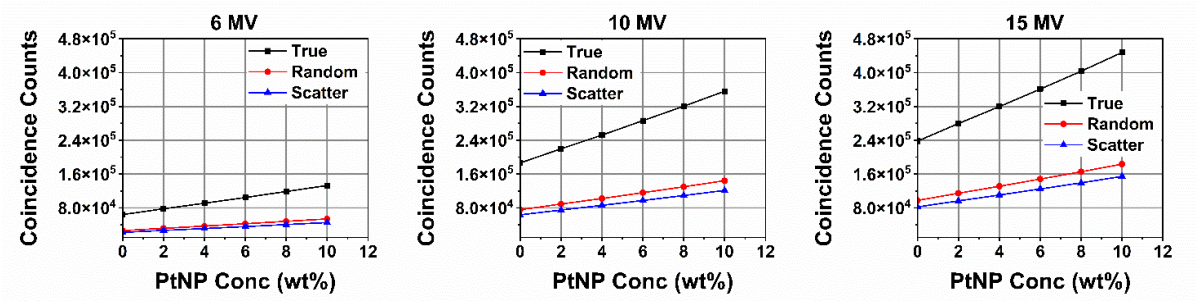

Figure 3. Variation in coincidence counts as a function of PtNP concentration in the MVIPET images.

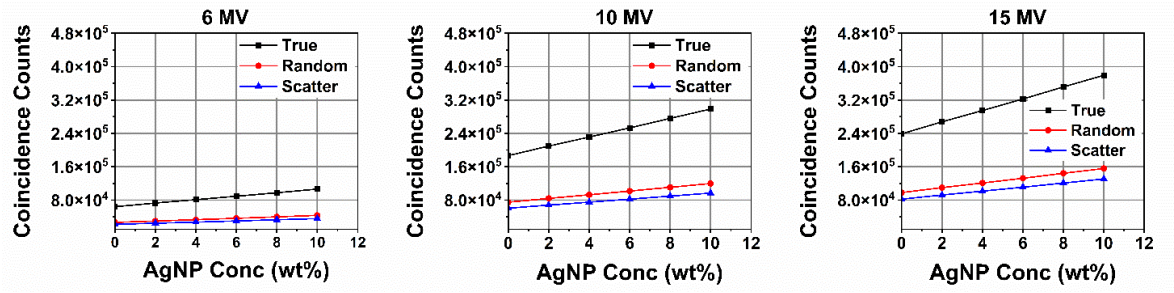

Figure 4. The variation of coincidence counts as a function of AgNP concentration in the MVIPET images

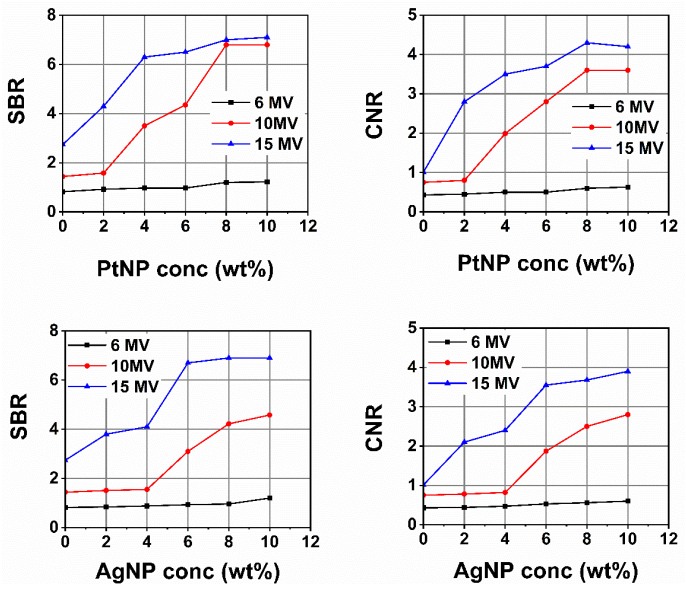

Figure 5. The variation of SBR and CNR as a function of PtNP and AgNP concentration in the MVIPET images

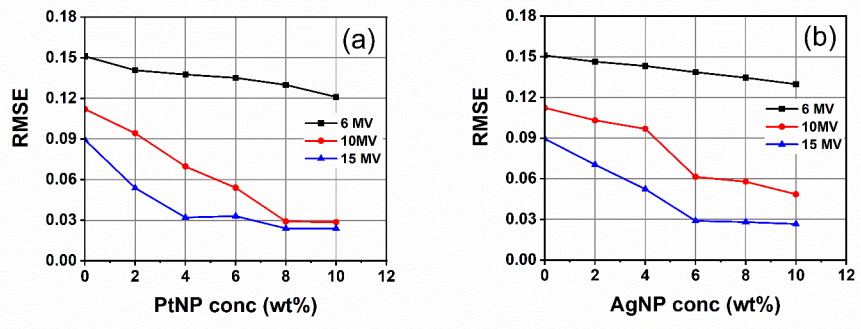

Figure 6. The values of RMSE as a function of PtNP (a) and AgNP (b) concentration and photon beam energy

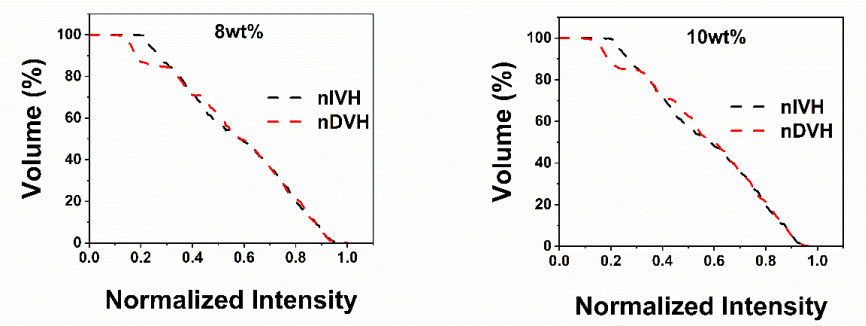

Figure 7. The nIVH and the nDVH in the lung tumoral tissue in the presence of PtNP at 8 and 10 wt% concentrations for a 10 MV photon beam.

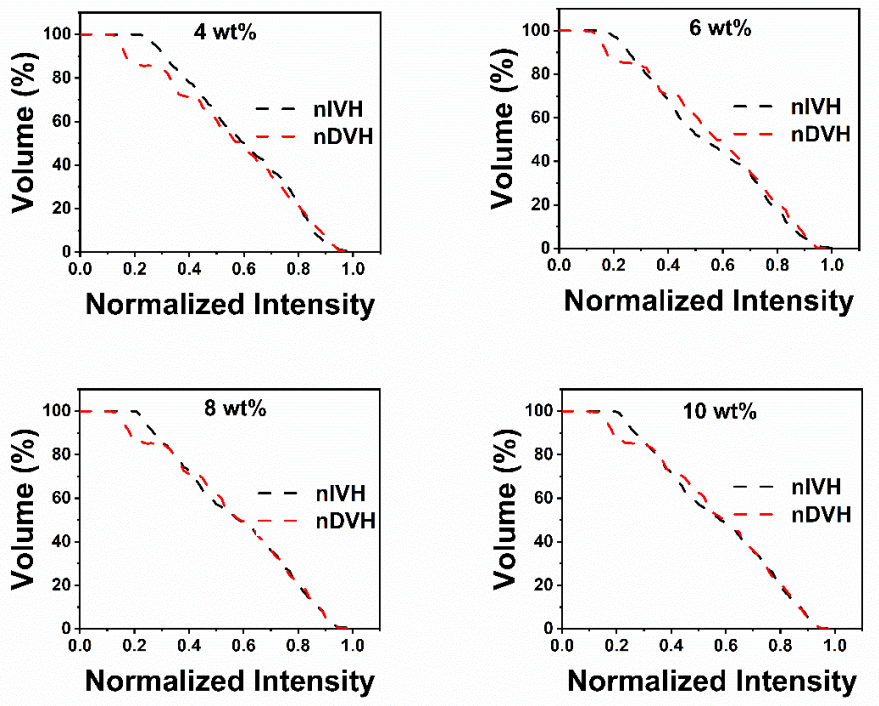

Figure 8. The nIVH and the nDVH in the lung tumoral tissue in the presence of PtNP with different concentrations for a 15 MV photon beam

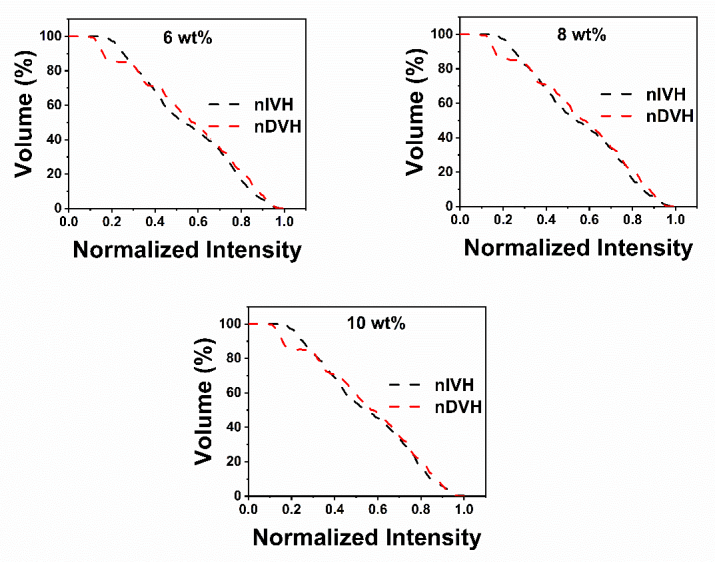

Figure 9. The nIVH and the nDVH in the lung tumoral tissue in the presence of AgNP with different concentrations for a 15 MV photon beam

Discussion

This study investigated the feasibility of detecting and quantifying annihilation photons emitted by lung tumors using AgNPs and PtNPs, which generate induced positrons. As shown in Figure 1(a), induced positrons increase with the NPs' atomic number (Z). The probability of pair production is enhanced in proportion to Z and photon energy [30]. Therefore, the intensity of 511 keV photons produced during positron annihilation was higher in the presence of PtNPs compared to AgNPs. Due to their high Z, dose-enhancement materials exhibit variations in mass attenuation coefficients and cross-sections, leading to dose enhancement. The interactions are explained by the photoelectric effect, Compton scattering, and pair production, with secondary electron generation contributing to dose enhancement [31]. For high-energy incident beams, pair production is a dominant interaction in high-Z materials, leading to a dose enhancement effect (Figure 2). On the other hand, a higher beam energy leads to greater pair production, generating more secondary electrons and increasing dose enhancement, consistent with Yu et al. [32]. This indicates that adding more NPs to the tumor leads to significant pair production. The mean absorbed tumor dose in the presence of PtNPs is significantly higher than in the presence of AgNPs, particularly for the 10 MV and 15 MV photon beams at higher concentrations.

The number of pair production interactions significantly affects the intensity of MVIPET images. As NP are introduced into the tumor, image contrast improves due to an increase in the probability of pair production. The pair-production cross-section is notably higher for Pt atoms at higher concentrations than for Ag atoms, making PtNPs more effective at enhancing tumor signal in imaging. As shown in Figure 3, the presence of PtNPs leads to higher total, true, scatter, and random coincidence counts compared to AgNPs. Additionally, SBR and CNR of reconstructed MVIPET images are notably enhanced with PtNPs, particularly at higher concentrations. However, as illustrated in Figure 4, the quality of MVIPET images obtained using either PtNPs or AgNPs is suboptimal, primarily due to the reduced positron production associated with the 6 MV beam. High-quality MVIPET images can be achieved when PtNP concentrations exceed 8 wt% and 4 wt% for 10 MV and 15 MV photon beams, respectively. This improvement is attributed to the increased positron production induced by 10 MV and 15 MV beams at higher NP concentrations. Images acquired in the presence of AgNPs using the 10 MV photon beam are of poor quality. However, acceptable image quality was observed for the 15 MV photon beam when the AgNP concentration exceeded 6 wt%. Lung tissue's low effective atomic number and density result in minimal attenuation of 511 keV photons. Additionally, lung tissue does not exhibit a significant Compton Effect. Furthermore, modern PET detectors use energy-window adjustments to filter out most non-pair photons. These factors contribute to a higher detection rate of 511 keV photons produced within the lung tumor.

The relationship between the reference dose and MVIPET-based dose was analyzed, as shown in Figures 6-9. The intensity of the MVIPET images increased with both photon energy and NP concentration, attributed to the greater number of positrons generated within the lung tumor. However, the RMSE values between the image-based nIVH and the reference nDVH remain elevated with increasing concentrations of both PtNPs and AgNPs under the 6 MV beam. This suggests that the images obtained with the 6 MV beam are unlikely to be suitable for dose monitoring. For 10 MV and 15 MV photon beams, the highest correlation between nIVH and nDVH (indicated by the lowest RMSE) was achieved at PtNP concentrations exceeding 4 wt% and 8 wt%, respectively, indicating that dose monitoring

during treatment is feasible under these conditions. In other words, the dose obtained from the MVIPET image can be reliable. In the presence of AgNPs, a minimum concentration of 6 wt% was required to enable dose monitoring, but only with the 15 MV photon beam. Since the tumor's absorbed dose and the MVIPET images' intensity are proportional to the fluence intensity, there will be a close correlation between the image pixel values and the reference absorbed dose. This relationship enables real-time dose monitoring through MVIPET images acquired during RT. Additionally, this approach verifies the radiation dose delivered to the patient.

In this study, NPs were assumed to be uniformly distributed within the lung tumor, while their presence in the surrounding lung tissue was neglected. This assumption was adopted due to computational constraints inherent to Monte Carlo simulations, as explicit modeling of individual NPs at nanometer scales within a macroscopic tumor volume is not feasible given the memory and computational requirements. Consequently, NPs were modeled using a homogenized material approach based on weight fraction, which is commonly employed in Monte Carlo dosimetric and imaging studies when the objective is macroscopic dose verification rather than nanometric track-structure analysis [17, 33].In reality, NP uptake is expected to be spatially heterogeneous across tissue types and within different tumor regions, potentially influencing positron production and, consequently, the intensity of the MVIPET signal. Such heterogeneity could affect the accuracy of the three-dimensional dose distribution derived from Monte Carlo simulations and the correlation between nIVH and nDVH. Therefore, further investigations incorporating spatially heterogeneous nanoparticle distributions in both tumor and surrounding tissues are warranted to more realistically assess their impact on MVIPET-based dose verification.

Conclusion

This study focused on examining the positrons induced through MVIPET in the presence of PtNPs and AgNPs to develop a method for estimating the in vivo radiation dose delivered to patients. Images were obtained by counting annihilation photons, similar to PET imaging. Increasing NP concentrations and the energy of the photon beam improved the quality of MVIPET images, enabling better discrimination between tumors and lung tissue. The values of SBR, CNR, and coincidence counts were determined based on Monte Carlo simulations and reconstructed images. When photon beams exceeding 10 MV were used, MVIPET image analysis indicated that lung tumors could be detected with this method, provided that NP were incorporated into the tumor. Furthermore, the improvement in image quality due to energy and NP concentrations was more significant for PtNPs than AgNPs. The findings of this study suggest that MVIPET is a promising method for real-time dose monitoring and verification during high-energy photon radiotherapy, especially for lung treatments. It is also compatible with standard PET-Linac systems.

References

1. Li Y, Yan B, He S. Advances and challenges in the treatment of lung cancer. Biomed Pharmacother. 2023;169:115891.
2. Ren XC, Liu YE, Li J, Lin Q. Progress in image-guided radiotherapy for the treatment of non-small cell lung cancer. World J Radiol. 2019;11(3):46-54.
3. Hansen CR, Hussein M, Bernchou U, Zukauskaite R, Thwaites D. Plan quality in radiotherapy treatment planning - Review of the factors and challenges. J Med Imaging Radiat Oncol. 2022;66(2):267-78.
4. Grégoire V, Guckenberger M, Haustermans K, Lagendijk JJW, Ménard C, Pötter R, et al. Image guidance in radiation therapy for better cure of cancer. Mol Oncol. 2020;14(7):1470-91.
5. Sakai Y, Monzen H, Takei Y, Kosaka H, Nakamura K, Yanagi Y, et al. Evaluation of In-room Volumetric Imaging Doses for Image-guided Radiotherapy: A Multi-institutional Study. J Med Phys. 2023;48(2):189-94.
6. Sun L, Gonzalez G, Pandey PK, Wang S, Kim K, Limoli C, et al. Towards quantitative in vivo dosimetry using x-ray acoustic computed tomography. Med Phys. 2023;50(11):6894-907.
7. Spinelli AE, Boschi F. Novel biomedical applications of Cerenkov radiation and radioluminescence imaging. Phys Med. 2015;31(2):120-9.
8. LaRochelle EPM, Shell JR, Gunn JR, Davis SC, Pogue BW. Signal intensity analysis and optimization for in vivo imaging of Cherenkov and excited luminescence. Phys Med Biol. 2018;63(8):085019.
9. Samant P, Trevisi L, Ji X, Xiang L. X-ray induced acoustic computed tomography. Photoacoustics. 2020;19:100177.
10. Kheruka SC, Jain A, Usmani MS, Al-Maymani N, Al-Makhmari N, Al-Saidi H, et al. Integrating Positron Emission Tomography Combined with Computed Tomography Imaging into Advanced Radiation Therapy Planning: Clinical Applications, Innovations, and Challenges. Journal of Medical Physics. 2025;50(2):198-206.
11. Brivio D, Sajo E, Zygmanski P. Gold nanoparticle detection and quantification in therapeutic MV beams via pair production. Phys Med Biol. 2021;66(6):064004.
12. Lyu Q, Neph R, Sheng K. Tomographic detection of photon pairs produced from high-energy X-rays for the monitoring of radiotherapy dosing. Nat Biomed Eng. 2023;7(3):323-34.
13. Berg E, Cherry SR. Innovations in Instrumentation for Positron Emission Tomography. Semin Nucl Med. 2018;48(4):311-31.
14. Kuncic Z, Lacombe S. Nanoparticle radio-enhancement: principles, progress and application to cancer treatment. Phys Med Biol. 2018;63(2):02tr1.
15. Liu W, Chen B, Zheng H, Xing Y, Chen G, Zhou P, et al. Advances of Nanomedicine in Radiotherapy. Pharmaceutics. 2021;13(11).

16. Jiang Z, Zhang M, Li P, Wang Y, Fu Q. Nanomaterial-based CT contrast agents and their applications in image-guided therapy. Theranostics. 2023;13(2):483-509.
17. Kumar PPP, Mahajan R. Gold Polymer Nanomaterials: A Promising Approach for Enhanced Biomolecular Imaging. Nanotheranostics. 2024;8(1):64-89.
18. Ahmad MY, Liu S, Tegafaw T, Saidi A, Zhao D, Liu Y, et al. Heavy Metal-Based Nanoparticles as High-Performance X-ray Computed Tomography Contrast Agents. Pharmaceuticals (Basel). 2023;16(10).
19. Talebi AS, Mehnati P, Rajabi H, Rezaei H, Geramifar P. Precision individual dosimetry in Yttrium-90 transarterial radioembolization in the presence of Au nanoparticles. Radiation Physics and Chemistry. 2024;222:111888.
20. McNutt TR, Mackie TR, Reckwerdt P, Paliwal BR. Modeling dose distributions from portal dose images using the convolution/superposition method. Med Phys. 1996;23(8):1381-92.
21. Sarrut D, Arbor N, Baudier T, Borys D, Etxebeste A, Fuchs H, et al. The OpenGATE ecosystem for Monte Carlo simulation in medical physics. Phys Med Biol. 2022;67(18).
22. Merlin T, Stute S, Benoit D, Bert J, Carlier T, Comtat C, et al. CASToR: a generic data organization and processing code framework for multi-modal and multi-dimensional tomographic reconstruction. Phys Med Biol. 2018;63(18):185005.
23. Zhu YM. Ordered subset expectation maximization algorithm for positron emission tomographic image reconstruction using belief kernels. J Med Imaging (Bellingham). 2018;5(4):044005.
24. Segars WP, Tsui BMW, Jing C, Fang-Fang Y, Fung GSK, Samei E. Application of the 4-D XCAT Phantoms in Biomedical Imaging and Beyond. IEEE Trans Med Imaging. 2018;37(3):680-92.
25. Sheikh-Bagheri D, Rogers DW. Monte Carlo calculation of nine megavoltage photon beam spectra using the BEAM code. Med Phys. 2002;29(3):391-402.
26. Levillain H, Burghelea M, Derijckere ID, Guiot T, Gulyban A, Vanderlinden B, et al. Combined quality and dose-volume histograms for assessing the predictive value of (99m)Tc-MAA SPECT/CT simulation for personalizing radioembolization treatment in liver metastatic colorectal cancer. EJNMMI Phys. 2020;7(1):75.
27. Hosseinabadi RB, Rajabi H. Real-time dosimetry in lung cancer radiotherapy using PET imaging of positrons induced by gold nanoparticles. Journal of Radiation Research and Applied Sciences. 2025;18(2):101361.
28. Siman W, Mawlawi OR, Mourtada F, Kappadath SC. Systematic and random errors of PET-based (90) Y 3D dose quantification. Med Phys. 2020;47(6):2441-9.
29. Siman W, Mawlawi OR, Mikell JK, Mourtada F, Kappadath SC. Effects of image noise, respiratory motion, and motion compensation on 3D activity quantification in count-limited PET images. Phys Med Biol. 2017;62(2):448-64.
30. Prasad SG, Parthasaradhi K, Bloomer WD. Effective atomic numbers of composite materials for total and partial interaction processes for photons, electrons, and protons. Med Phys. 1997;24(6):883-5.
31. Hwang C, Kim JM, Kim J. Influence of concentration, nanoparticle size, beam energy, and material on dose enhancement in radiation therapy. J Radiat Res. 2017;58(4):405-11.
32. Cheung JY, Ng BK, Yu KN. Dose enhancement close to platinum implants for the 4, 6, and 10 MV stereotactic radiosurgery. Med Phys. 2004;31(10):2787-91.
33. Talebi AS, Rajabi H, Watabe H. Role of nanoparticles in transarterial radioembolization with glass microspheres. Ann Nucl Med. 2022;36(5):479-87.